Egyptian Journal of Petroleum (2014) 23, 339–348

Egyptian Petroleum Research Institute

Egyptian Journal of Petroleum

www.elsevier.com/locate/egyjp
www.sciencedirect.com

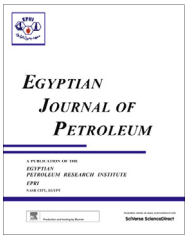

FULL LENGTH ARTICLE

Different outlet for preparing nano-TiO_2 catalysts for the photodegradation of Black B dye in water

Ahmed K. Aboul-Gheit, Doaa S. El-Desouki, Radwa A. El-Salamony *

Egyptian Petroleum Research Institute, Nasr City 11727, Cairo, Egypt

Received 21 July 2013; accepted 13 November 2013
Available online 13 October 2014

KEYWORDS

Amido black b dye;
Photodegradation;
Titanium isopropoxide;
Titanium tetrachloride

Abstract Two nano-titania catalysts were prepared using two economically varying titanium precursors: titanium tetrachloride (A) and titanium isopropoxide (B). The catalysts were calcined at temperatures of 500 °C, 600 °C and 700 °C and characterized using X-ray diffraction (XRD), electron diffraction (ED), BET surface properties and high resolution transmission microscopy (HRTEM). The calcined catalysts were found to differ markedly in their physical characters and TiO_2 phases produced as well as their photocatalytic activities. The anatase titania phase diminished from 100% to 83% in TiO_2A but from 64% to zero in TiO_2B via temperature increase from 500 °C to 700 °C, due to transforming anatase to rutile. The brookite TiO_2 phase only appeared (17%) in catalyst B500. In general, the catalyst of choice is A600 by virtue of many compositional, economical and catalytic advantages.

1. Introduction

TiO_2 semiconductor in nanoscale is considered as the most promising material for heterogeneous photocatalysis, due to its efficiency for eliminating organic pollutants and industrial residues in aqueous media [1,2]. The advantages of TiO_2 include powerful oxidation strength, high chemical stability, nontoxicity [3,4], photostability [5], high redox potential [6] and ability to produce electron/hole pairs with high life time and low cost [7] makes it a substantial oxide catalyst. Titanium dioxide has three crystalline phases: brookite (orthorhombic), anatase (tetragonal), and rutile (tetragonal). Rutile is the stable phase, whereas anatase and brookite are both metastable at all temperatures [8]. The energy band gaps are equal to 3.2 and 3.0 eV for anatase and rutile phases, respectively, which means that ultraviolet (UV) region of the solar spectrum is the proper region for the photoexcitation of TiO_2 nanoparticles to produce electron/holes and generation of OH radicals [9]. Many studies have indicated that the nanoparticles exhibit special photochemical characteristics [10] compared to the conventional larger particles. Also, the band gap of the nanoparticles increases with the decrease of particle size [11], and other important properties such as morphology, surface area, degree of crystallinity, anatase/rutile ratio which can be controlled during the preparation method and the heat treatment [12]. It has been disclosed that a 70/30% anatase/rutile in Degussa P-25 TiO_2 is conventionally selected as a reference photocatalyst for the oxidation of

* Corresponding author.
E-mail address: Radwa2005@hotmail.com (R.A. El-Salamony).
Peer review under responsibility of Egyptian Petroleum Research Institute.

http://dx.doi.org/10.1016/j.ejpe.2014.08.010

organics [13]. Several methods for TiO_2 nanoparticles preparation have been reported, such as chemical precipitation [14], microemulsion [15], hydrothermal crystallization [16] and sol–gel synthesis [17]. Many workers have studied the changes in morphology of TiO_2 with heat treatment. Porter et al. [18] studied microstructural changes in commercial Degussa P-25 TiO_2 due to heat-treatment. They found that with the increasing of calcination temperature the apparent crystallite size and rutile content in the catalyst increased, whereas the specific surface area and the rate of phenol photodecomposition under UV irradiation decreased. The same effect was observed by Reddy et al. [19]. Inagaki et al. [20] characterized TiO_2 powders obtained by titanium tetraisopropoxide (TTIP) hydrolysis that is annealed in the range from 400 °C to 900 °C for different periods of time. A marked increase in the crystallite size and a decrease in lattice strain were observed for catalysts annealed above 600 °C. The rate of methylene blue degradation in UV increased with increasing calcination temperature of the catalyst from 400 °C to 700 °C. Calcination of the precursors above 700 °C is indicated by a smaller rate constant, mainly due to partial transformation of anatase to rutile [20].

Azo dyes are the largest group of synthetic colorants (60–70%) and are being used in industry for applications such as textiles, papers, leathers, gasoline, additives, foodstuffs, cosmetics, laser materials, xerography, laser printing, etc. Only 45–47% dye stuffs have been reported to be biodegradable due to their insolubility [21]. Because of the toxicity and persistence of azo dyes, their removal from the wastewater has become an important issue of interest during the last few years.

In the present work, TiO_2 nano powder was prepared via two different techniques; sol–gel technique using TTIP as a precursor in acidic medium and precipitation technique using titanium tetrachloride ($TiCl_4$) as a cheaper precursor in basic medium, all at various calcination temperatures, for the purpose of preparing a more impressive nano TiO_2 photodegradative catalyst for organic dye in aqueous medium.

2. Experimental

2.1. Catalyst preparation

Titanium tetrachloride ($TiCl_4$, 15%) was used as a precursor for preparing nanosized TiO_2 powder by *precipitation method* [22] using ammonia solution as precipitating agent and ethanol as dispersing agent. 25 ml $TiCl_4$ was dissolved in 20 ml distilled water in an ice-water bath. The titanium solution was then slowly mixed with 30 ml distilled water and 20 ml ethanol under vigorous stirring, then ammonia solution was added drop-wise until pH = 9. During the ammonic addition, an intensive precipitation occurred. After the solvent was evaporated at 80 °C for 24 h, the precipitates were dried at 300 °C for 2 h to remove NH_4Cl, then calcined in an air stream at 500 °C, 600 °C and 700 °C for 4 h, hence the catalysts were named A500; A600 and A700, respectively.

A second method for TiO_2 nanoparticle preparation "*sol–gel method*" [23] was used where $Ti(OH)_4$ sol was prepared by mixing 5 ml titanium tetraisopropoxide ($Ti(OCH(CH_3)_2)_4$, 99.5%, Aldrich) with 50 ml isopropanol (Adwic, A.R.) under vigorous stirring. The mixture was then allowed to undergo partial hydrolysis at room temperature by drop-wise addition of 5 ml isopropanol and 2 ml hydrochloric acid (pH = 3–4) with constant stirring. $Ti(OH)_4$ gel was dried at 100 °C overnight then calcined in an air stream at 500 °C, 600 °C or 700 °C for 4 h each. These catalysts were named B500, B600 and B700, respectively.

2.2. Photocatalytic degradation procedure

The degradation of azo dye black b was employed in the current study as an indication for the prepared nano TiO_2 solid catalyst activity parameter. The chemical structure of the dye is illustrated herein.

Photodegradation was carried out in air using Pyrex glass made reactor containing 500 ml of the dye solution. The photocatalyst was maintained in suspension by magnetic stirring. In all experiments, air was bubbled continuously through the suspension. The suspension was irradiated with an UV 254 nm (8 W) lamp. All experiments were performed at 25 ± 1 °C. A previously determined optimum concentration of TiO_2 in suspension was 0.5 g L^{-1}, while the dye concentration was 25 ppm in all experiments. The suspension was first stirred in the dark for 30 min to reach the equilibrium adsorption. During both dark adsorption and UV-irradiation periods, samples of 5 ml were collected every hour and filtrated. The discoloration was monitored by measuring the absorbance at λ_{max} = 615 nm, using JENWAY-6505 UV–visible spectrophotometer. Each experiment was carried out for 5 h. Moreover, the pseudo-first-order rate constant (k, h^{-1}) for the photocatalytic degradation of black-b was determined by Eq. (1) [24]:

$$\ln\frac{C}{C_0} = kt \tag{1}$$

The k value was calculated from a plot of $\ln(C_0/C)$ *vs.* irradiation time (t), where C_0 and C denote the black-b concentrations at $t = 0$ and t = t, respectively. The pseudo-first-order rate constant was used as an indicator for evaluating the photocatalytic activity of the synthesized TiO_2 photocatalysts.

2.3. Physical characterization of the catalysts

The specific area of all nano TiO_2 catalysts was measured using the BET technique under N_2 gas to validate surface area and texture characterization changes with the preparation conditions. Surface area, pore volume and pore size distribution were evaluated using NOVA2000 gas sorption analyzer (Quantachrome Corporation) system. For each measurement,

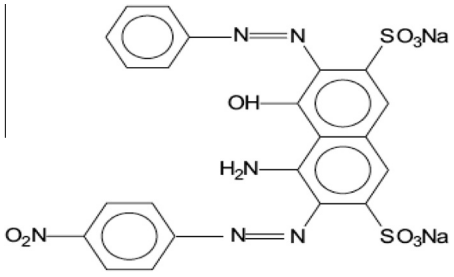

Scheme 1 Chemical structure of Amido black 10 b dye.

the sample was degassed at 250 °C for 3–4 h then analyzed at 77 K. The surface areas and pore volumes were determined using the adsorption branch in the relative pressure range of 0.05–0.35. The pore volume distribution of the samples was calculated from the nitrogen uptake at $P/P_o = 0.95$ using the DFT (Density Functional Theory) method from the isothermal desorption data.

XRD analysis was performed to determine the rutile and anatase concentrations in each TiO_2 sample. X-ray powder diffraction (XRD) patterns were obtained using PANalytical X'Pert PRO diffractometer in reflection mode using CuK_α radiation over the scan range of 2θ between 20 and 80 at 295 K.

Crystallite size (D) of the photocatalysts was calculated from the line broadening of X-ray diffraction peak according to the Scherrer formula (Eq. (2))

$$D = \frac{K\lambda}{\beta\cos(\theta)} \tag{2}$$

where K is the Scherrer constant (0.89), λ is the wavelength of the X-ray radiation (0.15418 nm for CuK_α), β is the full width at half maximum (FWHM) of the diffraction peak measured at 2θ, where θ is the diffraction angle.

The morphology of the dry powder as well as electron diffraction (ED) patterns was investigated using transmission electron microscopy (TEM) using a JEOL 2100F TEM at an accelerating voltage of 200 kV. Prior to the analysis, the catalyst sample was ground into powder then ultrasonically dispersed in water and placed on a carbon-coated copper grid.

3. Results and discussion

3.1. Structure characterization of solid catalysts

3.1.1. XRD analysis

According to environment and preparation conditions, TiO_2 can exist in three crystalline phases, namely; anatase, rutile and brookite, where the titanium ion coordinates with six oxygen atoms in each form. Anatase and rutile are tetragonal, while brookite is orthorhombic. Anatase and brookite are relatively thermodynamically unstable and transform at high calcination temperatures to rutile [25].

Fig. 1(a and b) represents the XRD patterns of the nano TiO_2 calcined from both precursors at 500 °C, 600 °C and 700 °C where highly crystalline solid is manifested. With increasing the temperature from 500 °C up to 700 °C, the diffraction peaks become narrower, which indicates crystal lattice expansion [25]. Also from Scherrer equation [26], the mean crystallite size of TiO_2 is found to increase as the calcination temperature increases (Table 1). These results agree with those of Chen and Tao [27] who suggested that the growth process of nanocrystalline anatase is due to single crystal sintering within the agglomerates, and finally the original agglomerate transforms to a larger single crystal.

The phase content in the powders has been calculated from integrated intensities of anatase (1 0 1), rutile (1 1 0) and brookite (1 2 1) peaks represented by A_A, A_R and A_B, respectively. The mass fraction of rutile (W_R), anatase (W_A) and brookite (W_B) was calculated from Eqs. (3a), (3b) and (3c) where K_A and K_B are coefficients with values 0.886 and 2.721 [28];

$$W_A = \frac{K_A A_A}{K_A A_A + A_R + K_B A_B} \tag{3a}$$

$$W_R = \frac{A_R}{K_A A_A + A_R + K_B A_B} \tag{3b}$$

$$W_B = \frac{K_B A_B}{K_A A_A + A_R + K_B A_B} \tag{3c}$$

The obtained X-ray diffraction results are listed in Table 1 showing that at calcination temperature 500 °C, catalysts A give only anatase phase diffraction peaks (referring to JCPDS Card Number 04-001-7641) which can be observed in the XRD pattern at $2\theta = 25.31°$, 37.81° and 48.11°, while a weak peak at around 27.5° appears in the pattern of sample A600 (5%) and increases in sample A700 (19%). These results agree with those of Zheng et al. [29]. However, in catalysts B, the sample calcined at 500 °C (B500) shows, beside the anatase diffraction peaks, those relevant to rutile (referring to JCPDS Card Number 00-034-0180) appearing at $2\theta = 27.5°$, 36.5°, 41.0°, 54.1° and 56.5° as well as brookite phase (referring to JCPDS Card Number 00-003-0380) which appears in somewhat lower intensity at $2\theta = 30.81°$. Therefore the percentages of anatase, rutile and brookite comprise 64%, 19% and 17%, respectively. It has been observed that the brookite phase decreases with increasing calcination temperature whereas the rutile phase increases such that the sample calcined at 700 °C (B700) contains absolutely rutile phase. This indicates that the transformation of anatase to brookite is a transition step to form rutile. Hence, it can be concluded that the transformation temperature from anatase phase to the rutile phase in catalysts of group A starts at 600 °C whereas, it is $\leqslant$500 °C in case of catalysts. Kamal et al. [30] also found that the transformation temperature of the crystal prepared by sol–gel is in the range of 500−650 °C which indicates that the crystal type is not only related to the thermal treating temperature but also to the preparing methods and raw materials.

Fig. 1a and b shows the electron diffraction (ED) patterns for catalysts of groups A and B, respectively. As calcination temperature increases, the crystallized fraction, ED patterns as well as intensity of XRD peaks are increased. All SAED patterns for TiO_2 nanoparticles show polycrystalline particles [31]. The A500 sample shows ring patterns of anatase phase without any diffraction rings of second phase which is in agreement with XRD results. Moreover, the d-spacing (lattice spacing) from XRD is 0.35 nm for 1 0 1 plane, which corresponds to the anatase TiO_2 crystalline structure [32]. Also, the d-spacing of rutile phase is 0.32 nm for 1 1 0 plane in A600 and A700 samples. Catalysts B show more crystallinity where the rings in SAED are sharper and more spotty.

3.1.2. Surface characteristics

All isotherms in the present investigation, obtained for catalysts A and B of prepared TiO_2, belong to type IV isotherms which are associated with capillary condensation in mesopores where the limiting uptake is over a range of high P/P_o. The initial part of type IV isotherms can be attributed to monolayer-multilayer adsorption.

The behavior of A catalysts show isotherms that can be said to belong to the H3 loop subclass of the type IV isotherms since it does not exhibit any limiting adsorption at high $P/P°$ values. More definitely, the adsorption isotherms obtained for B catalysts evidently show hysteresis loops that are typically belonging to H2 isotherms of the type IV

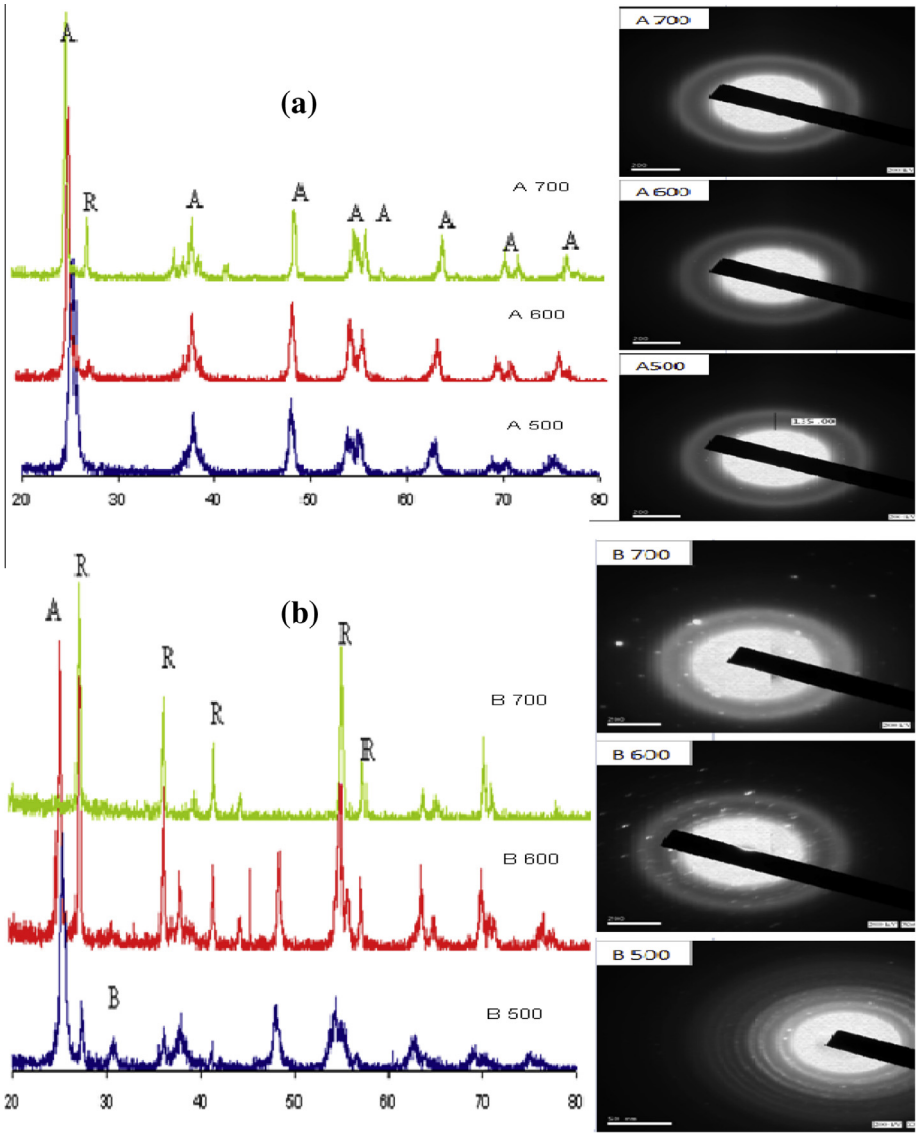

Figure 1 XRD analysis and ED patterns of TiO_2 catalysts.

Table 1 Textural and structural properties of TiO_2 samples.

Samples	Phase ratio[a]			Crystal size[a] (nm)			Specific surface area[b] (m^2/g)	Pore radius Dv (r)[c] (nm)	Total pore volume [c] (cc/g)
	A	R	B	D_A	D_R	D_B			
A 500	100	0	0	28.5	–	–	69.5	4.1	0.271
A 600	95	5	0	16.6	17.3	–	54.3	6.9	0.325
A 700	83	17	0	37.8	46.4	–	46.6	6.9	0.19
B 500	64	19	17	17.1	34.3	9.7	61.3	3.1	0.135
B 600	52	48	0	25.8	32.1	–	21.7	3.9	0.061
B 700	0	100	0	–	34.4	–	0.08	6.4	0.025

[a] According to XRD analysis.
[b] BET surface area calculated from the linear portion of the BET plot in the relative pressure range of $p/p_0 = 0.05–0.35$.
[c] Pore radius and total pore volume estimated using DTF method from the isothermal desorption data.

(particularly samples B500 and B600), whereas sample B700 tends to belong more effectively to class H1 of type IV for which the two branches are nearly parallel and steeper than the H2 isotherms obtained for samples B500 and B600 isotherms is steeper than their adsorption branch. The type H3 loop (Fig. 2b), which does not exhibit any limiting adsorption at high $P/P°$ indicates the presence of aggregates of plate like particles giving rise to skit-shaped pores. The use of $TiCl_4$ as a Ti precursor for preparing the less expensive TiO_2 catalyst (catalysts A) is an obvious case of this type of loop structure production. However, type H2 loop (Fig. 2a) gives narrow pore size distribution.

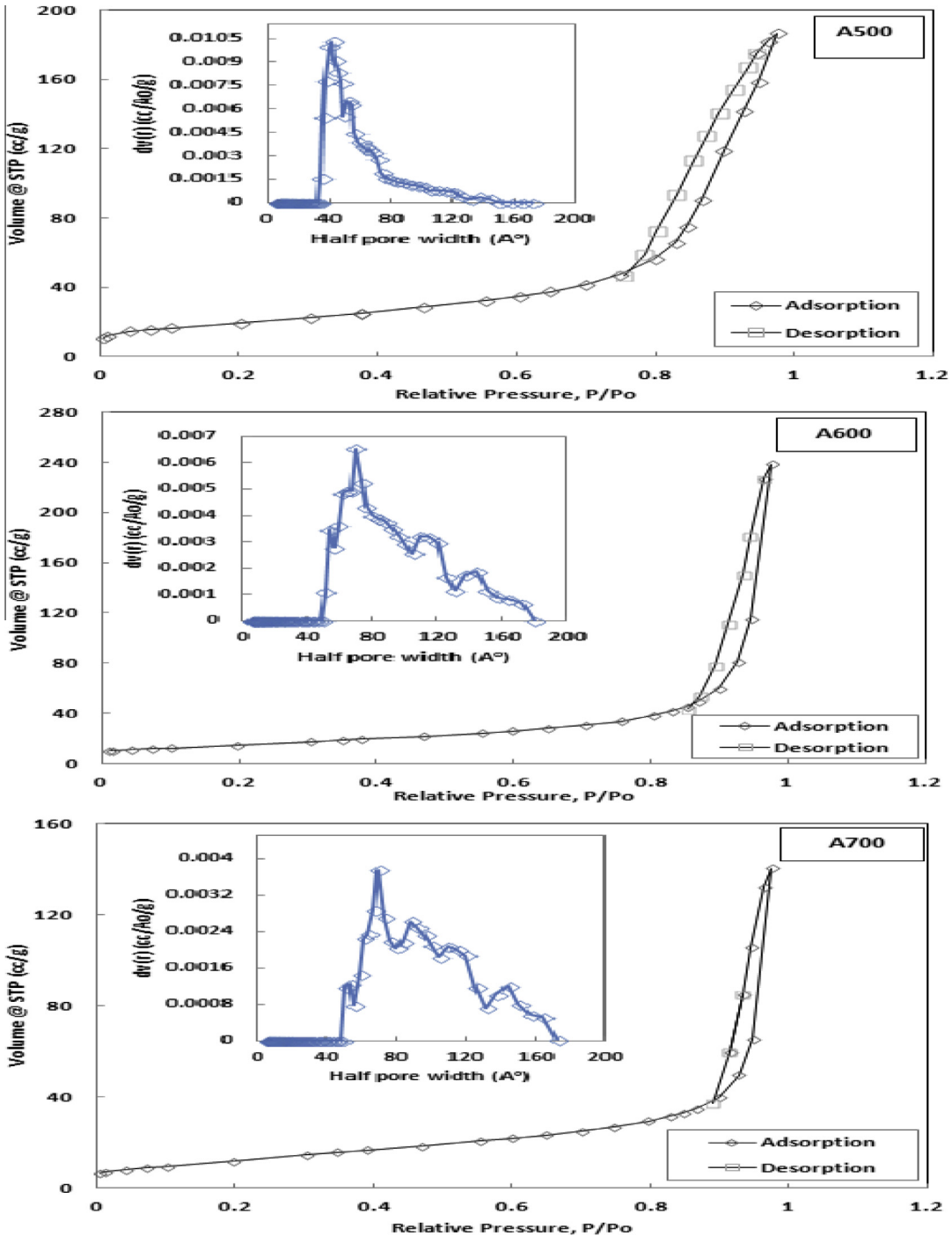

Figure 2a Nitrogen adsorption/desorption isotherms at 77 K for TiO_2 synthesized from $TiCl_4$ precursor and calcined at 500 °C, 600 °C, 700 °C.

The BET surface area obtained for TiO_2 prepared using titanium tetrachloride (catalysts A) is much higher than that of alkoxide-derived powders (catalysts B) (Table 1). This is compatible with the finding of Zhang et al. [33].

Pore volume distribution of the TiO_2 catalysts prepared using $TiCl_4$ as a precursor is shown in Fig. 2a. The total pore volume in the A500 catalyst version amounts to 0.271 cc/g. We have applied the DFT method which magnifies the behavior of the pore volume distribution in the region above 8 up to 32 nm. Sample A500 shows a maximum pore volume at 8.2 nm beyond which gradual decrease of this distribution occurs as pore volume increases to ~32 nm. Correspondingly; the A600 and A700 samples show close similarity of their pore volume distribution. This distribution in both samples increases to a maximum at ~12 nm then decreases representing cascading steps with maxima at around 14, 23, 29 and 36 nm. The total pore volume in these samples amounts to 0.325 and 0.190 cc/g, respectively. The catalyst exhibiting the highest

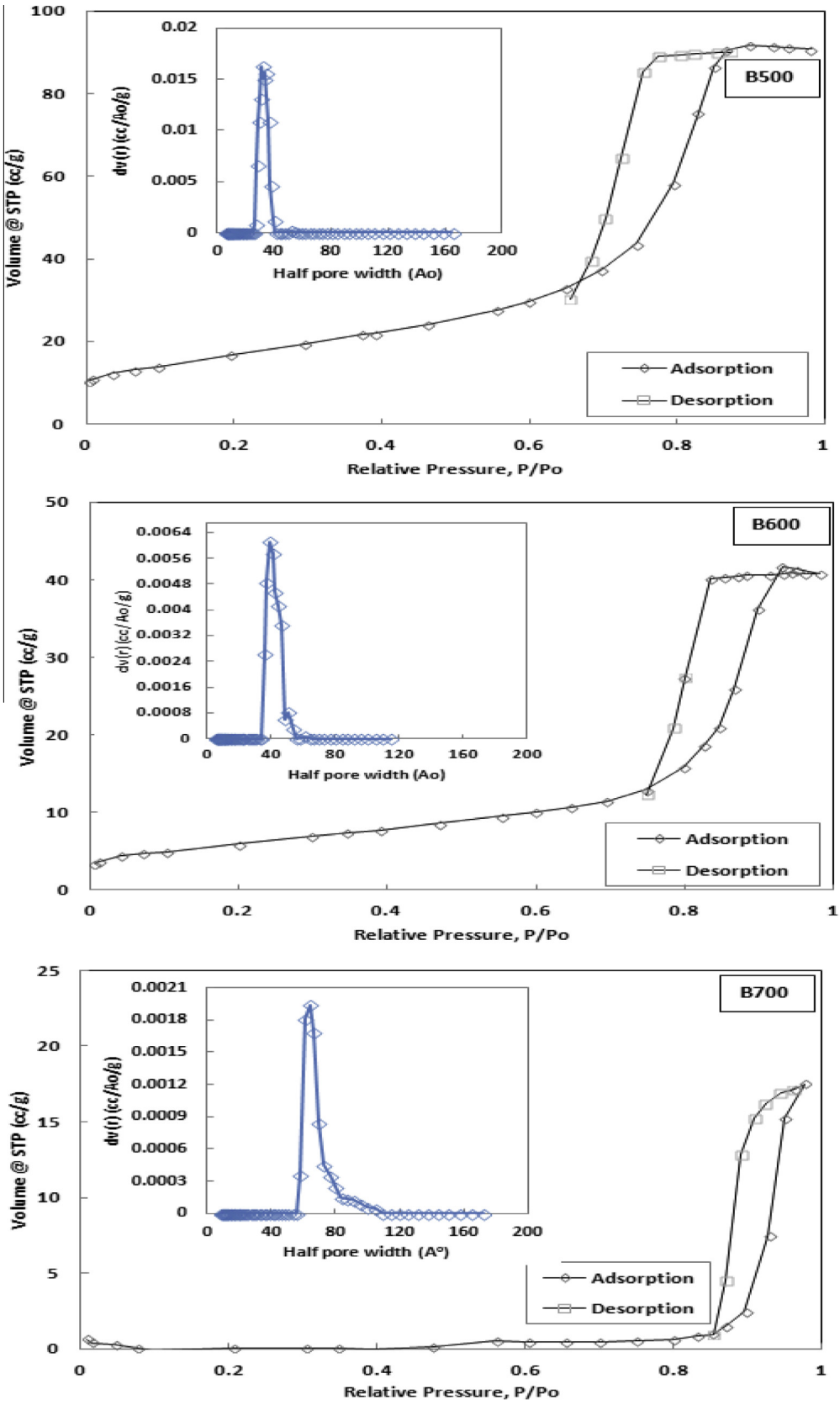

Figure 2b Nitrogen adsorption/desorption isotherms at 77 K for TiO_2 synthesized from TTIP precursor and calcined at 500 °C, 600 °C, 700 °C.

pore volume is found to acquire the highest photocatalytic degradation activity. Although the pore volume distribution of the A600 and A700 samples exhibits close similarity, the former one acquires higher activity due to its larger pore volume and adequate TiO_2 composition which is similar to that of the standard TiO_2 Degussa P25. Nevertheless, the A700 sample exhibits significant amount of larger crystallite size of both anatase phase (37.8 nm) and rutile phase (46.4 nm) compared to those in sample A600 amounting to 16.5 nm for anatase and 17.3 nm for rutile.

On the other hand, the pore volume distribution in catalysts of group A shows a wider range of pore width (8–34 nm) than in catalysts of group B. However, in both cases, the pore distribution gets more and more wider with increasing the calcination temperature. Particularly in case of group A catalysts, where it is found that in A500 sample, the range falls between 8 and 24 nm; in A600 and A700 samples in the range 8–35 nm. The distribution curves of B group catalysts are much narrower with maxima at 6.2, 7.8 and 12.8 nm using the B500, B600, and B700, respectively, i.e., the pores in these catalysts get wider as the calcination temperature becomes higher. The B500 catalyst acquires the highest pore volume in this group, i.e., 0.135 cc/g, compared to 0.061 and 0.025 cc/g for the B600 and B700 catalysts, respectively. Furthermore, the rutile content is 48% and 100%, respectively, which deviates excessively, show that acquired by standard P25 catalyst. On the contrary, the B500 catalyst has optimum rutile content (19%). It is to be observed that the overall pore size values are smaller for B500 and increase with increasing temperature (Fig. 2b). Moreover dv(r) values are in the order B500 > B600 > B700.

3.1.3. TEM

Fig. 3 shows the transmission electron microscopic (TEM) bright field images for the TiO_2 nanopowders prepared using $TiCl_4$ as precursor (catalysts A), the TEM analysis was carried out to confirm the actual size of the agglomerated particles. The average size of particles is ~20 nm which is in agreement with that of XRD measurements. Under very high resolutions, we can recognize that the shape of the particles changes from semi-sphere (A500) to more sharp particles as the calcination temperature increases. The larger cubic-shaped particles are crystallites of rutile. The equilibrium between the nucleation and the growth makes the formation of TiO_2 particles in the rutile possible, and the morphology of rutile is cubic-shaped. Similar findings have been encountered by Slunecko et al. [34]. However, the TEM photographs taken for catalyst B calcined at 500 °C and 600 °C show reasonable uniformity of crystallinity, whereas for the B700 catalyst sample, strong agglomeration appears to take place.

3.2. Photodegradation of black b dye

3.2.1. Effect of catalyst precursor

Fig. 4 shows the effect of calcination temperature (500 °C, 600 °C, 700 °C) on the photocatalytic degradation of black b dye using photocatalysts A and B. The pore volume is mostly related to the diffusion of pollutants during the photocatalytic reaction, i.e., the higher the pore volume of the catalyst, the more effective the diffusion of pollutants in the catalyst. Guo et al. [35] reported similar data on the photocatalytic activity of mesoporous TiO_2.

Obviously, the A600 catalyst gives the highest photodegradation activity of the black b dye compared with the other catalysts (A500, A700) showing that a temperature of 600 °C is an optimum calcination temperature using the current economic precursor material (Fig. 4). The proportion of smaller pores in the A500 catalyst (8–16 nm) is evidently much larger than in the A600 and A700 catalysts, which causes more diffusion limitation of the dye molecules. However, although the pore distribution curves for A600 and A700 samples are similar with respect to acquiring higher proportions of wider pores (16–34 nm) than in A500 sample, it can thus be assumed that the lower photoactivity of A700 than A600 is principally attributed to its higher proportion of the rutile form compared to the anatase form.

According to Eq. (1), the linear relationship of $\ln(C/C_0)$ with respect to the irradiation time suggested the first-order kinetics, where the apparent rate constant k_{app}, according to activity, is found to be 0.069, 0.121, 0.734 and 1.000 h^{-1} using the B500, A500, A700 and A600 catalysts, respectively (Fig. 5).

The data in Table 1 show the change of rutile as a TiO_2 compositional component in the current catalysts as a function of calcination temperature. Evidently, rutile is increased on the expense of anatase with temperature; at 500 °C, rutile is completely absent whereas at 600 °C and 700 °C, rutile fraction amounts to 5 and 17, respectively. However, in group B catalysts, rutile is 19% at 500 °C and increases to 48% at 600 °C then reaches 100% at 700 °C. The effect of rutile formation with increasing calcination temperature should not be ignored, since the higher photoactivity appearing using the A600 catalyst can be attributed to the limited production of rutile to be associated with anatase that causes a delay of recombination of electron and hole on the catalyst surface during the photo reaction.

Also, Bickley et al. [36] reported the enhanced light absorption activity of the mixed phases and suggested the transfer of photo generated electrons from a lower energy rutile to anatase electron site. This electron transfer would serve to reduce the recombination rate of anatase by increasing the separation between the electron and hole, resulting in greater catalytic reactivity. Furthermore, many catalytic "hot spots" may be located at the solid–solid interface of anatase and rutile, which is favorable for the improvement of photocatalytic activity [37]. However; Liu et al. [38] indicated that a higher content of rutile can possess abundant surface water and hydroxyl groups, and hence a high photocatalysis efficiency.

The calcined version at 700 °C (A700), although acquires the lowest pore volume and lowest surface area but acquires a more adequate percentage of rutile (19%) gives a photoactivity slightly lower than that of the A600 catalyst which is the most active one. This may be at least partially attributed to its highest adsorption capacity (Fig. 4) and most proper rutile content. Several investigators have observed that there is a clear relationship between substrate adsorbability and photocatalytic degradation [39]. However, this rutile ratio is comparable to Degussa P25 catalyst which has been considered as a reference for the photodegradation of organic pollutants [40].

In this study, the peaks at wave lengths of 300 nm in Fig. 6, are attributed to (UV) absorbance characteristic of adjacent aromatic rings in the current dye, whereas the visible band at 610 nm is characteristic of long conjugated systems internally linked by two azo groups [41]. Hence, the peak at 300 nm is related to the degradation of the aromatic ring whereas the

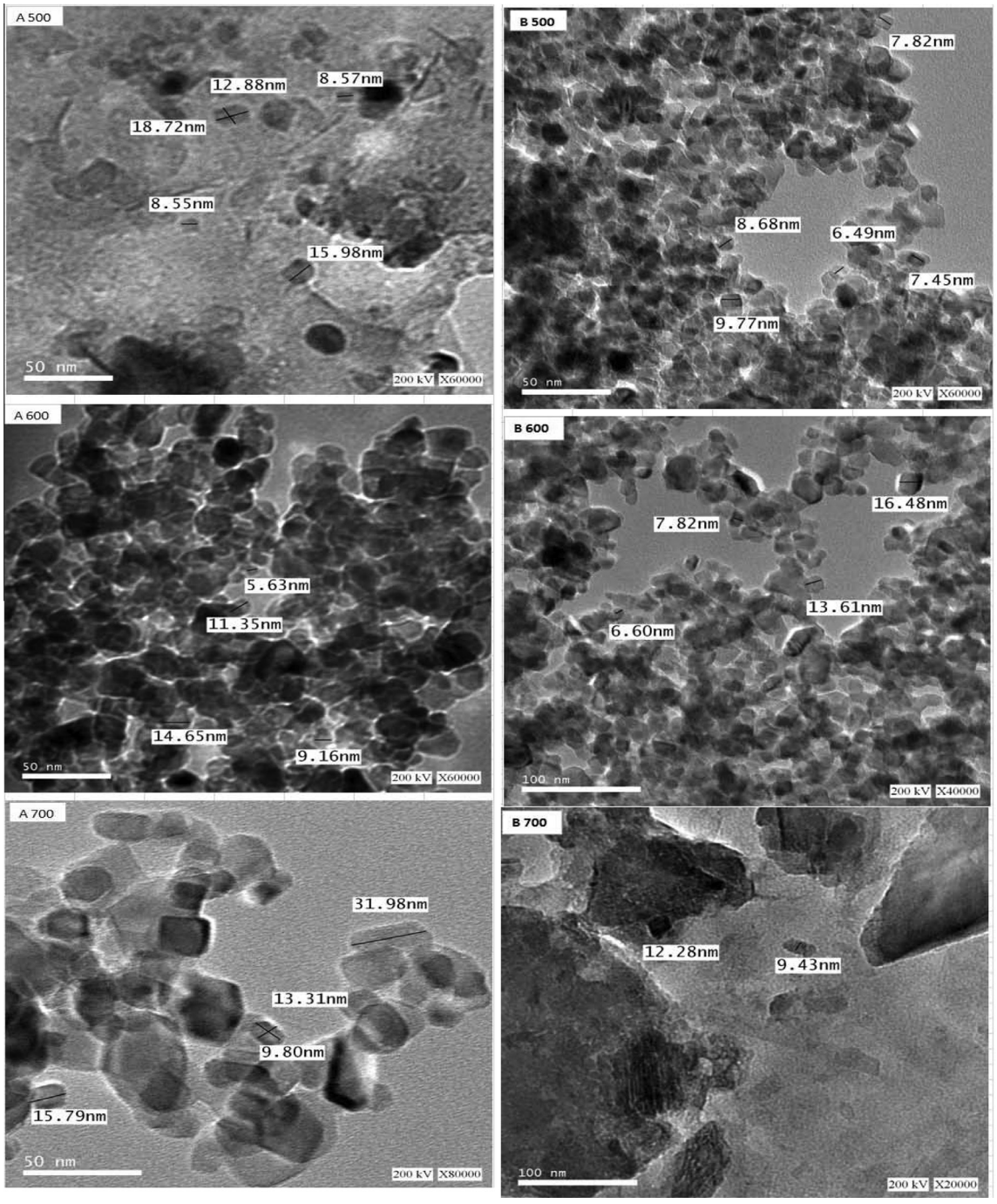

Figure 3 TEM images for A500, 600, 700 and B500, 600, 700 catalysts.

peak at 610 nm is related to the coloring absorption. As shown in Fig. 6, with further irradiation time increase continuous decreasing of both absorbance bands occurs till complete degradation and decolonization. It is evident that both absorbance bands at 300 and 610 nm decrease with approximately the same rate as a function of irradiation time. This may ascertain that our A600 catalyst is active for both the degradation of azo groups as well as for destroying the aromatic structures in the dye. However; Yu et al. [40] found that the rate of decolorization is ~1.4 times higher than the rate of aromatic ring degradation in reactive black 5 dye using the Degussa P25.

3.2.2. Effect of dye concentration

The initial concentration of the dye is of practical importance since it is related to the quantity of the dye adsorbed on the surface of the photocatalyst. The extent of dye adsorption depends on the initial dye concentration. The degradation efficiency decreases with increasing the amount of dye concentration (Figs. 7 and 8). This can be explained on the basis of the assumption that on increasing the dye concentration, more organic substances are adsorbed on the surface of TiO_2 where less number of photons are available to reach the catalyst surface and hence less $^{\bullet}OH$ radicals are produced [42]. Qamar et al. reported that [43] for the Amido black 10 b dye, the

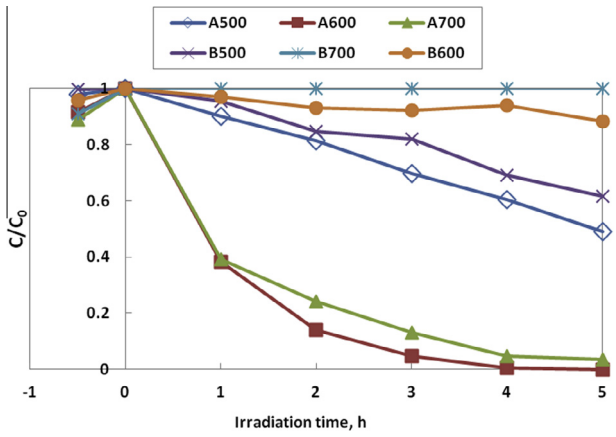

Figure 4 Photocatalytic degradation of black-b dye using A and B catalyst groups at different calcinations temperatures.

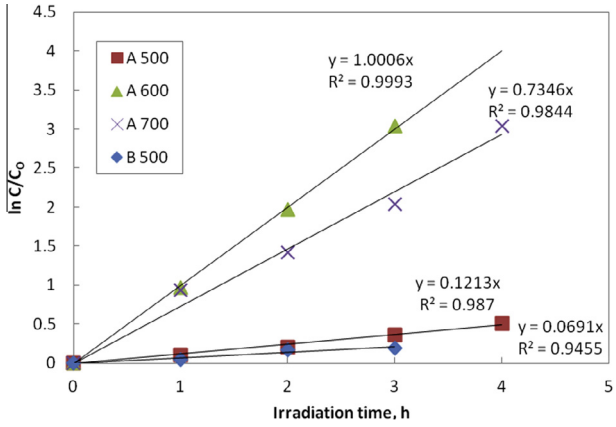

Figure 5 Apparent first-order kinetics for the corresponding photocatalytic reaction.

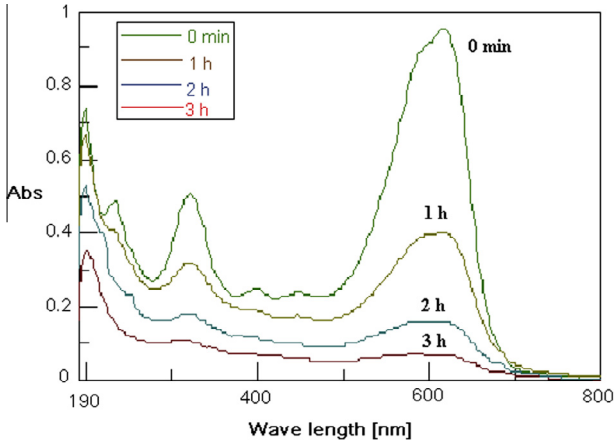

Figure 6 UV–vis spectral changes of black b using A600 catalyst under UV irradiation.

degradation rate was found to decrease continuously with the increase in substrate concentration from 0.25 to 0.75 mM. The black b dye photodegradation rate is found to increase as a function of decreasing the dye concentration in water (Fig. 7). Furthermore, Fig. 8 shows a first order plot ($\ln C/C_o$ *vs time*) as shown by the high R^2 accuracy factor.

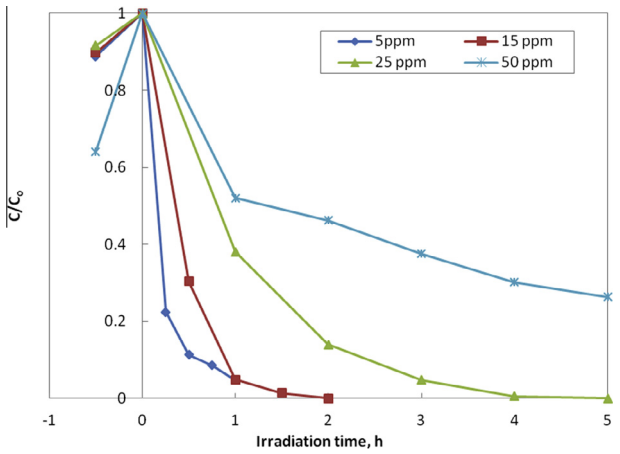

Figure 7 Effect of initial dye concentrations on photocatalytic degradation process using A600 catalyst under UV irradiation.

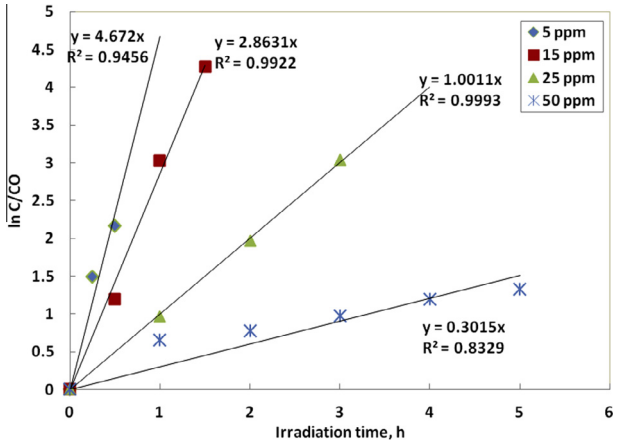

Figure 8 Apparent first-order kinetics for the corresponding photocatalytic reaction.

3.2.3. Photocatalytic kinetics

Different kinetic models have been proposed in order to characterize the photodegradation reaction [44]. In most of the above studies, Langmuir–Hinshelwood model was applied to describe the photodegradation rate expression in terms of the disappearance of compounds [45]. Fig. 9 shows the variation of black b dye reciprocal initial concentration versus reciprocal of reaction rate using the A600 and A700 catalysts according to the simplified form Eq. (4):

$$\frac{1}{r_0} = \frac{1}{k} + \frac{1}{kK} \cdot \frac{1}{C_0} \tag{4}$$

where k denotes the reaction rate constant for the process, K is the adsorption coefficient of reactants, C_0 is the initial concentration of the black b dye and r_0 is the initial rate of the reaction. Accordingly, a linear relationship between $1/r_0$ and $1/C_0$ is represented in Fig. 9. The value of intercept evaluates $1/k$ and the slope corresponds to $1/kK$.

The reaction rate constant, k obtained for the photodegradation of the current dye using A600 catalyst is 0.83 mg h^{-1} (Fig. 9), whereas using the A700 catalyst k amounts to 0.34 mg h^{-1}. Even though, the adsorption coefficient K calculated using the latter catalyst is found to be 0.029 Lm g^{-1} while

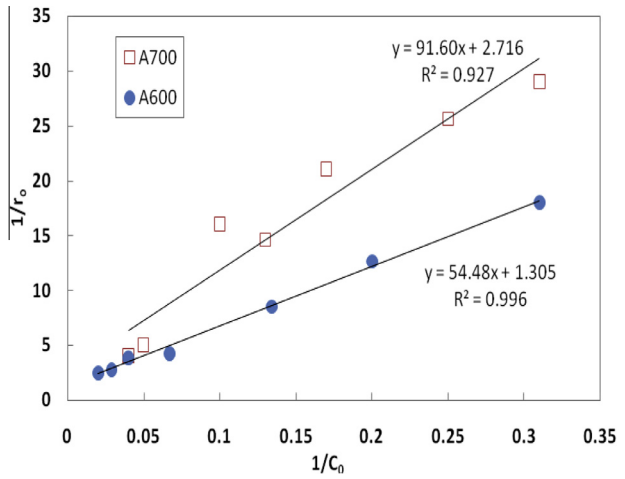

Figure 9 Linear correlation of $1/r_0$ versus $1/C_0$.

using the former catalyst K is 0.0215 Lm g^{-1}. In other words, the catalytic photodegradation activity of TiO_2, although lower using the A700 catalyst, its adsorptive coefficient is higher. Hence, in the present case, such higher adsorptivity can be said to unfavor activation of the catalyst, i.e., exerts some inhibition. This can be also attributed to the relatively complicated molecule of the dye shown in Scheme 1 where stronger adsorption of the dye on the catalyst surface can be inhibiting.

4. Conclusion

This work shows that the photocatalytic activity of nano-TiO_2 for black b dye degradation is more effective on using $TiCl_4$ as a Ti-precursor for preparation of nano-TiO_2 catalyst compared to the more expensive Ti-tetraisopropoxide precursor. The A600 catalyst exhibits the highest activity. This catalyst is composed of 95% anatase and 5% rutile and acquires the highest total pore volume (0.325 cc/g). The activity data are well supported by TEM, XRD, ED and surface characterizations.

References

[1] D.W. Bahnemann, S.N. Kholuiskaya, R. Dillert, A.I. Kulak, A.I. Kokorin, Appl. Catal. B: Environ. 36 (2002) 161.
[2] L.R. Skubal, N.K. Meshkov, T. Rajh, M. Thurnauer, J. Photochem. Photobiol. A: Chem. 184 (2002) 393.
[3] P. Zhang, S. Yin, T. Sato, Appl. Catal. B 89 (2009) 118–122.
[4] A.R. Liu, S.M. Wang, Y.R. Zhao, Z. Zheng, Mater. Chem. Phys. 99 (2006) 131.
[5] W. Smith, A. Wolcott, R.C. Fitzmorris, J.Z. Zhang, Y. Zhao, J. Mater. Chem. 21 (2011) 10792–10800.
[6] M.G. Bawendi, M.L. Steigerwald, L.E. Brus, Annu. Rev. Phys. Chem. 41 (1990) 477–496.
[7] A. Fujishima, K. Hashimoto, T. Watanabe, TiO_2 Photocatalysis: Fundamentals and Applications, Bkc, Tokyo, 1999.
[8] X.Z. Ding, X.H. Liu, J. Mater. Sci. Lett. 15 (1996) 1789–1791.
[9] A. Sclafani, L. Palmisano, M. Schiavello, J. Phys. Chem. 94 (1990) 829–832.
[10] T. Torimoto, H. Kontani, Y. Shibutani, S. Kuwabata, T. Sakata, H. Mori, H. Yoneyama, J. Phys. Chem. B 105 (2001) 6838.
[11] M. Addamo, V. Augugliaro, A. Di Paola, E. Garciá-Lpez, V. Loddo, G. Marcí, R. Molinari, L. Palmisano, M. Schiavello, J. Phys. Chem. B 108 (2004) 3303–3310.
[12] D. Bersani, G. Antonioli, P.P. Lottici, T. Lopez, J. Non-Cryst. Solids 232–234 (1998) 175–218.
[13] R.J. Berry, M.R. Mueller, J. Microchem. 50 (1994) 28.
[14] S. Jeon, P.V. Braun, Chem. Mater. 15 (2003) 1256–1263.
[15] Y. Bessekhouad, D. Robert, J.W. Veber, J. Photochem. Photobiol. A: Chem. 157 (2003) 47–53.
[16] Y.V. Koleńko, B.R. Churagulov, M. Kunst, L. Mazerolles, C.C. Justin, Appl. Catal. B: Environ. 54 (2004) 51–58.
[17] X. Wang, G. Wu, B. Zhou, J. Shen, Materials 6 (2013) 2819–2830.
[18] J.F. Porter, Y. Li, C.K. Cahn, J. Mater. Sci. 34 (1999) 1523–1531.
[19] K.M. Reddy, C.V.G. Reddy, S.V. Manorama, J. Solid State Chem. 158 (2001) 180–186.
[20] M. Inagaki, R. Nonaka, B. Tryba, A.W. Morawski, Proceedings of 4th International Conference Oils and Environment AUZO 2005, June 20–23, Gdansk, Poland (2005), pp. 325–332.
[21] Ö. ÇInar, S. Yasar, M. Kertmen, K. Demiröz, N.Ö. Yigit, M. Kitis, Process Saf. Environ. Prot. 86 (2008) 455–460.
[22] X. Jiang, G. Ding, L. Lou, Y. Chen, X. Zheng, Catal. Today 93–95 (2004) 811–818.
[23] B. Pal, M. Sharon, J. Mol. Catal. A: Chem. 160 (2000) 453–460.
[24] A.K. Aboul-Gheit, S.M. Abdel-Hamid, S.A. Mahmoud, R.A. El-Salamony, J. Valyon, M.R. Mihályi, Á. Szegedi, J. Mater. Sci. 46 (2011) 3319–3329.
[25] C.S. Barret, T.B. Massalski, Mc Graw-Hill series in materials science and engineering, 1966.
[26] P. Scherrer, G. Nachrichten, Math. Phys. 2 (1918) 98–100.
[27] W. Chen, X. Tao, J. Zhang, Q. Fang, J. Yang, J. Am. Ceram. Soc. 88 (2005) 2998–3002.
[28] H. Zhang, J.F. Banfield, J. Phys. Chem. B 104 (2000) 3481–3487.
[29] R. Zheng, Y. Guo, C. Jin, J. Xie, Y. Zhu, Y. Xie, J. Mol. Catal. A: Chem. 319 (2010) 46–51.
[30] A.M. Kamal, V. Srinnivas, E.P. Sotiris, AIChE J. 40 (1994) 1183–1188.
[31] R.S. Sonawane, M.K. Dongare, J. Mol. Catal. A: Chem. 243 (2006) 68–76.
[32] M.J. Velasco, E. Ocana, J.L. Rubio, Bol. Soc. Esp. Ceram. Vidrio 33 (1994) 259.
[33] Q. Zhang, L. Gao, J. Guo, J. Eur. Ceram. Soc. 20 (2000) 2153–2158.
[34] J. Slunecko, M. Kosec, J. Holc, G. Drazic, J. Am. Ceram. Soc. 81 (1998) 1121–1124.
[35] B. Guo, H. Shen, K. Shu, Y. Zeng, W. Ning, J. Chem. Sci. 121 (2009) 317–321.
[36] R. Bickley, T.G. Carreno, J. Lees, J. Solid State Chem. 92 (1991) 178–190.
[37] G.H. Li, L. Chen, M.E. Graham, K.A. Gray, J. Mol. Catal. A: Chem. 275 (2007) 30–35.
[38] G. Liu, X. Wang, Z. Chen, H.M. Chen, G.Q. Lu, J. Colloid Interface Sci. 329 (2009) 331–338.
[39] V. Subramanian, V.G. Pangarkar, A.A. Beenackers, Clean Prod. Processes 2 (2000) 149–156.
[40] C.H. Yu, C.H. Wu, T.H. Ho, P.K. Andy Hong, Chem. Eng. J. 158 (2010) 578–583.
[41] R.M.C. Silverstein, G.C. Basdler, G.C. Morrill, Spectrophotometric Identification of Organic Compounds, Wiley, New York, 1991.
[42] C.C. Wang, C.K. Lee, M.D. Lyu, L.C. Juang, Dyes Pigm. 76 (2008) 817–824.
[43] M. Qamar, M. Saquib, M. Muneer, Dyes Pigm. 65 (2005) 1–9.
[44] A.J. Julson, F.D. Ollis, Appl. Catal. B: Environ. 65 (2006) 315–325.
[45] C. Hana, Z. Li, J. Shen, J. Hazard. Mater. 168 (2009) 215–219.